ADVANCED MATERIALS
www.advmat.de

Switching Vertical to Horizontal Graphene Growth Using Faraday Cage-Assisted PECVD Approach for High-Performance Transparent Heating Device

Yue Qi, Bing Deng, Xiao Guo, Shulin Chen, Jing Gao, Tianran Li, Zhipeng Dou, Haina Ci, Jingyu Sun, Zhaolong Chen, Ruoyu Wang, Lingzhi Cui, Xudong Chen, Ke Chen, Huihui Wang, Sheng Wang, Peng Gao, Mark H. Rummeli, Hailin Peng, Yanfeng Zhang, and Zhongfan Liu**

Plasma-enhanced chemical vapor deposition (PECVD) is an applicable route to achieve low-temperature growth of graphene, typically shaped like vertical nanowalls. However, for transparent electronic applications, the rich exposed edges and high specific surface area of vertical graphene (VG) nanowalls can enhance the carrier scattering and light absorption, resulting in high sheet resistance and low transmittance. Thus, the synthesis of laid-down graphene (LG) is imperative. Here, a Faraday cage is designed to switch graphene growth in PECVD from the vertical to the horizontal direction by weakening ion bombardment and shielding electric field. Consequently, laid-down graphene is synthesized on low-softening-point soda-lime glass (6 cm × 10 cm) at ≈580 °C. This is hardly realized through the conventional PECVD or the thermal chemical vapor deposition methods with the necessity of high growth temperature (1000 °C–1600 °C). Laid-down graphene glass has higher transparency, lower sheet resistance, and much improved macroscopic uniformity when compare to its vertical graphene counterpart and it performs better in transparent heating devices. This will inspire the next-generation applications in low-cost transparent electronics.

The direct metal-catalyst-free growth of graphene on insulating substrates, such as SiO_2,[1,2] Al_2O_3,[3,4] $SrTiO_3$,[5] and glass,[6,7] is critical to the development of graphene-based electronics, which bypasses the complicated graphene transfer procedure and accordingly avoids severe film quality degradation.[2,8–11] However, for high-quality graphene synthesis on insulating substrates through conventional thermal chemical vapor deposition (CVD) method, high growth temperature (1000–1600 °C) is always necessary to assist the decomposition of carbon precursors and boost the crystallization of graphene.[2,3,5,7] This synthetic process is cost ineffective because of high energy consumption. Furthermore, the choices of substrates are generally limited to high-temperature-resistant

Y. Qi, B. Deng, T. R. Li, H. N. Ci, Z. L. Chen, R. Y. Wang, L. Z. Cui, X. D. Chen, K. Chen, H. H. Wang, Prof. H. L. Peng, Prof. Y. F. Zhang, Prof. Z. F. Liu
Center for Nanochemistry (CNC)
Academy for Advanced Interdisciplinary Studies
Beijing National Laboratory for Molecular Sciences
College of Chemistry and Molecular Engineering
Peking University
Beijing 100871, China
E-mail: yanfengzhang@pku.edu.cn; zfliu@pku.edu.cn

X. Guo, Prof. S. Wang
Key Laboratory for the Physics and Chemistry of Nanodevices
Department of Electronics
Peking University
Beijing 100871, China

S. L. Chen, Z. P. Dou, Prof. P. Gao
Electron Microscopy Laboratory
School of Physics
Center for Nanochemistry (CNC)
Peking University
Beijing 100871, China

J. Gao
Institute of Functional Nano and Soft Materials (FUNSOM)
Soochow University
Suzhou, Jiangsu 215006, P. R. China

Prof. J. Y. Sun
Soochow Institute for Energy and Materials Innovations (SIEMIS)
Key Laboratory of Advanced Carbon Materials and Wearable Energy Technologies of Jiangsu Province
Soochow University
Suzhou, Jiangsu 215006, P. R. China

Prof. M. H. Rummeli
Soochow Institute For Energy and Materials Innovations (SIEMIS)
School of Energy
College of Physics
Optoelectronic and Energy
Soochow University
Suzhou, Jiangsu 215006, P. R. China

Prof. H. L. Peng, Prof. Y. F. Zhang, Prof. Z. F. Liu
Beijing Graphene Institute (BGI)
Beijing 100095, China

Prof. Y. F. Zhang
Department of Materials Science and Engineering
College of Engineering
Peking University
Beijing 100871, P. R. China

DOI: 10.1002/adma.201704839

materials, such as Al_2O_3 and SiO_2, whereas other universal materials with low softening/melting point, e.g., soda-lime glass (<600 °C) are hardly applicable. Therefore, reducing the growth temperature of graphene is imperative.

Plasma-enhanced chemical vapor deposition (PECVD) is a reliable and scalable route for the low-temperature synthesis of graphene (<600 °C) on insulating substrates, owing to its capability of generating active species in plasma (e.g., charged particles, energetic electrons, free radicals, and photons).[12–15] Interestingly, graphene obtained through this method is typically shaped like vertical nanowalls, named vertical graphene (VG)-nanowalls, which possess rich exposed edges, large specific surface area, nonstacking morphology, and good out-of-plane conductivity.[16] These specifics endow VG-nanowalls wide applications in biosensor,[17] supercapacitor[18] as well as energy storage and conversion.[19]

However, for VG-nanowalls, the in-plane conductivity was not ideal due to serious scattering of charge carriers at the abundant exposed edges.[20–23] The unique vertical structures could also function as "optical traps," resulting in increased light absorption and degraded transparency.[7,24–27] The applications of such graphene nanowalls in transparent electronics were thus limited to some extent. The laid-down graphene (LG)-layers could better overcome the above issues, hence are more suitable for transparent electronic applications. It is highly desirable to synthesize LG-layers on transparent insulating substrates (e.g., glass), through an innovative low-temperature PECVD route.

The intense ion bombardment and directional electric field are two main factors to induce the formation of VG-nanowalls during a PECVD reaction.[14,28–33] In the initial stage of graphene growth, the ion bombardment and lattice mismatch between substrate and graphitic material usually caused defects and buckles in the buffer layers, followed with the accumulation of internal stress.[14,32] Accordingly, the edges of buffer layers or defects curved upward, and the vertical growth of graphene stemmed from these curving edges.[34] Subsequently, the diffusion of carbon cations along the vertical nanowalls was enhanced by the local electric field in the sheath layer in plasma, which guided the vertically oriented growth of graphene.[14,32,35,36]

Herein, a copper-foam-based Faraday cage was designed to weaken the ion bombardment and shield the electric field, aiming for switching graphene growth in PECVD from vertical to horizontal directions. With the Faraday-cage-assisted PECVD method, three goals have been achieved: (1) Graphene synthesis on glass was realized at the temperature below the softening temperature of soda-lime glass (≈580 °C), and the initial morphology of glass was maintained, which is hardly achieved using the thermal CVD method with the necessity of high growth temperature (1000–1600 °C); (2) Lateral growth of graphene was resulted in the PECVD system, which is not possible through the conventional PECVD method with the typical product of VG-nanowalls, and the LG-layers possess higher transparency and lower sheet resistance comparing with the VG-nanowalls counterpart, making it more suitable for transparent electronic applications; (3) Large-scale uniform synthesis of graphene was derived in the designed PECVD system due to the elimination of electric field distortion effect around the glass edges in the Faraday cage, and the thickness uniform region (up to 6 cm × 10 cm) is larger than the normal PECVD-derived one. The laid-down graphene on glass performs excellently in transparent heating devices, which sheds light on their applications in next-generation low-cost transparent electronics.

The photograph and schematic of the PECVD apparatus are displayed in Figure S1a,b in the Supporting Information. The utilized plasma source is the direct current (dc) glow discharge type. Methane (CH_4) accompanied by argon (Ar) and hydrogen (H_2) is introduced into the chamber through the showerhead placed on the upper side. A mass spectrum of ions revealed that the main ions in plasma included three categories: hydrogen related (H^+, H_2^+, H_3^+), argon related (Ar^+, Ar_2^+, ArH^+), and carbon related (CH_x^+, $C_2H_x^+$, $C_3H_x^+$, $C_4H_x^+$) ones. The neutral species such as H, H_2, H_3, Ar, Ar_2, CH, CH_2, and CH_3, were also detected.[15,37,38]

Under normal PECVD growth route, i.e., exposing the substrate directly in plasma, the carbon pieces deposited on the substrate form buffer layers at the initial growth stage. The impurities on the substrate, the defects produced by intense ion bombardment, and the lattice mismatch between substrate and adlayer induce the accumulation of internal stress in buffer layers, which leads to curl up of the defect or layer edges. This is where the vertical growth of graphene stems from (procedures (1) in **Figure 1**a). In the subsequent growth process, the local electric field in the sheath layer in plasma drives the charged carbon species to move alongside the vertical nanowalls until reaching the curled edges, and covalently bond to the edge atoms (procedures (2) in Figure 1a). Additionally, owing to the stronger localized electric field at the sharp VG-nanowall edges, the atmospheric carbon cations would preferentially land at the nanowall edges to participate graphene growth. This electric field enhancement at the edges of nanowalls has also been used in corona discharge electrodes.[39] The whole process for the vertical growth of graphene is schematically depicted in Figure 1a, according to the published references.[14,29,32,34–36]

To evaluate the distribution of electric field in such a PECVD system, a 2D qualitative simulation is carried out (Figure 1c). The simulated length and height of the chamber and the glass substrate are 1:1 to the objects, with values of 15 cm (length) × 5 cm (height) and 5 cm × 0.1 cm, respectively. As a result, most of the space in chamber presents nearly uniform electric field with a magnitude of ≈6000 V m^{-1}, except for the spaces around the glass edges.

After the normal PECVD growth process, a rough surface usually evolved, as presented in Figure S2 in the Supporting Information by corresponding scanning electron microscopy (SEM) and atomic force microscopy (AFM) images. The magnified AFM image (Figure 1e) presents a typical VG-nanowall structure, with a room mean square (RMS) roughness of ≈10.5 nm and nanowall height of ≈40.1 nm (growth duration: ≈10 min). Figure 1f is the cross-sectional transmission electron microscope (TEM) image for VG-nanowalls on glass, which presents the vertical-oriented morphology of graphene.

However, as mentioned above, in transparent electronic applications, the degradation of transmittance[25–27] and conductivity[20–23] always occurs in VG-nanowall-based samples. The synthesis of LG-layers in PECVD is therefore preferential to overcome such issues. Considering the electric field effect in plasma, a natural idea is to shield it by a unique Faraday cage. In

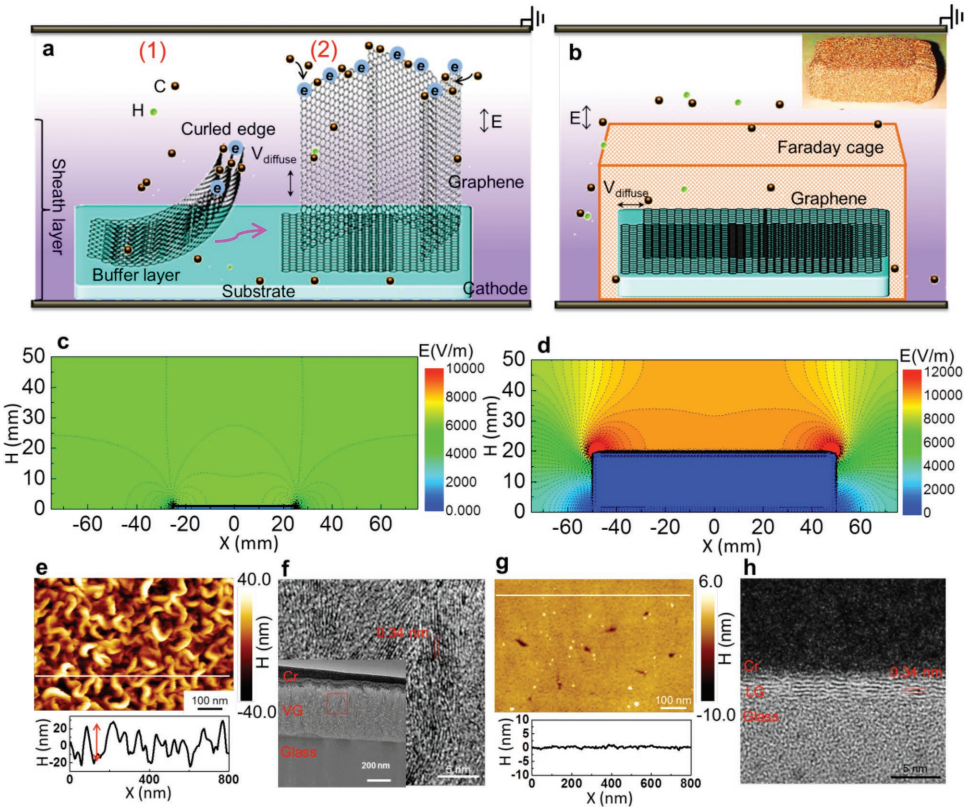

Figure 1. VG-nanowalls and LG-layers growth on glass in the PECVD system. a,b) Schematics and mechanisms for the normal and Faraday-cage-assisted PECVD growth routes. Inset in (b): Photograph for the copper-foam-based Faraday cage with size of 15 cm (length) × 10 cm (width) × 2 cm (height). c,d) 2D simulated distributions of the electric field in PECVD without c) and with d) Faraday cage under the voltage of 300 V. The dashed lines represent the contour lines of the equal-magnitude electric field. The simulated length and height of reaction chamber, glass, and Faraday cage are 15 cm (length) × 5 cm (height), 5 cm × 0.1 cm, and 10 cm × 2 cm, respectively, and the simulated aperture size of Faraday cage is 0.5 mm. e) AFM image of VG-nanowalls on glass with an RMS roughness of ≈10.5 nm (growth time: ≈10 min). Bottom height profile along the line presents a nanowall height of ≈40.1 nm (red arrow). g) AFM image of LG-layers on glass with an RMS roughness of ≈0.4 nm (growth time: ≈60 min). Bottom height profile along the line displays the flat surface. f,h) Cross-sectional TEM images for VG-nanowalls f) and LG-layers h) on glass, respectively. Inset in (f): Large-scale cross-sectional TEM image for VG-nanowalls.

this respect, the Faraday cage is constructed with the commercial copper foam, which possesses an aperture size of ≈0.5 mm and porosity of ≈80%. The size of the Faraday cage is 15 cm (length) × 10 cm (width) × 2 cm (height) (inset photograph in Figure 1b), which is hollow with the glass putting inside.

On one hand, this copper-foam-based Faraday cage enables the partial blockage of incident energetic particles reaching the glass surface, thereby mitigating the ion bombardment effect and reducing the defects produced in the buffer layers. The internal stress, which induces the upward curling of the edges of defects, would be accordingly weakened.[14,32] On the other hand, when Faraday cage is utilized in the PECVD system, an electric field lower than 0.1 V m^{-1} can be realized, as simulated in Figure 1d (aperture size: 0.5 mm). In this regard, the electric-field effect inducing the vertical growth of graphene is greatly suppressed. The plasma redistribution surrounding the Faraday cage is shown in the on-site photo in Figure S1c in the Supporting Information.

Consequently, the Faraday-cage-shielded graphene glass possesses a large-scale surface flatness (Figure S2c, Supporting Information), featured by a much smaller RMS roughness of ≈0.4 nm, as shown in Figure 1g. The as-produced flat lying geometry was further convinced by transferring onto an SiO_2/Si substrate, showing a film thickness of ≈1.1 nm (Figure S3, Supporting Information) (growth time: ≈60 min). Figure 1h is the cross-sectional TEM image for LG-layers on glass, which addresses the laid-down morphology of graphene.

In the previous studies,[40,41] Faraday cage has been applied in the plasma etching process to eliminate the distortion of electric field at the convex corner of microfeatures on substrate, aiming to suppress the faceting and achieve the vertical etching profile. Note that, our work herein represents the first report to apply the electric field shielding effect of Faraday cage in material synthesis to switch graphene growth in PECVD from vertical to horizontal directions. Interestingly, this Faraday-cage-assisted PECVD route successfully realizes the low-temperature (≈580 °C) synthesis of LG-layers on catalysis-free insulating substrate. This is hardly realized through the conventional PECVD method with the typical product of VG-nanowalls, or the thermal CVD method with the necessity of high growth temperature (1000–1600 °C).

In the synthesis of VG-nanowalls and LG-layers on glass via PECVD, the nanowall height, layer thickness, and surface roughness of obtained graphene could be tailored by adjusting

the growth durations (see Figures S4 and S6, Supporting Information for details). These varied morphologies of graphene could impose different surface wettability on glass. The contact angles of VG nanowall-covered glass with different nanowall height and surface roughness are displayed in Figure S7a in the Supporting Information. As such, the bare glass shows a pristine static water contact angle of ≈30.8°, whereas the VG nanowall-covered glass becomes highly hydrophobic with the contact angle larger than 130°. In contrast, LG layer-covered glass shows much smaller contact angle, which could be tailored between 67.9° and 98.7° by adjusting the growth time (Figure S7b, Supporting Information). It is evident to observe that VG nanowall-covered glass shows superior hydrophobicity as compared to the LG layer-covered glass.

In light of the scalable applications of graphene glass in transparent electronics, its large-scale uniformity is a key prerequisite. In the present work, Faraday cage performs excellently in improving the uniformity. To clarify this issue, the distribution of electric field surrounding the glass in PECVD was carefully evaluated through the 2D theoretical simulation. With regards to a normal PECVD system, an uneven distribution of the electric field (from ≈6000 to ≈8000 V m^{-1}) on the glass surface can be observed, with the positions changing from the internal areas to the edges (**Figure 2**a). This could be explained by the fact that the equipotential contour in the sheath layer in plasma is curved following the microfeatures on the substrate surface, including the edges and the sharp points. A concentrated electric field was usually induced at the convex corner due to its high aspect ratio.[40,41] Herein, for glass directly exposed to the plasma, the flux of carbon cations around the edges is obviously increased by this field distortion, as compared with that at the internal areas, giving rise to a higher growth rate of graphene, and consequently the formation of thicker graphene at glass edges.

The macroscopic photograph, transmittance measurement, AFM characterization, and Raman spectroscopy were used to evaluate the uniformity of graphene glass. The photograph of normal PECVD-derived graphene glass (Figure 2c)

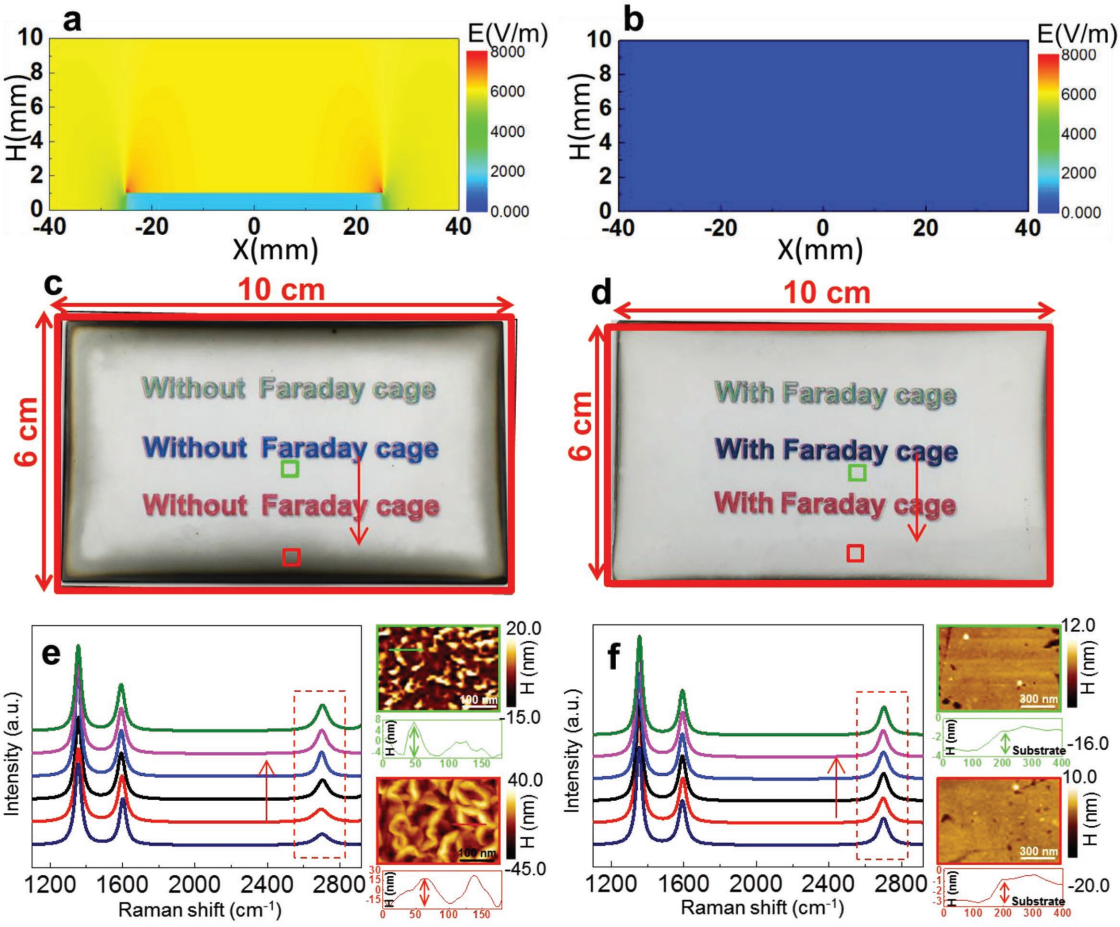

Figure 2. Uniformity comparisons between graphene glasses obtained through the normal and Faraday-cage-assisted PECVD routes. a,b) 2D simulated distributions of the electric field around the glass directly in plasma a) and in Faraday cage b) (just presenting the inner space of the cage, aperture size: ≈0.1 mm). c) Photograph of normal PECVD-derived graphene glass (10 cm × 6 cm), with the transmittance of ≈30.5% at glass edges and ≈80.0% at the central regions. d) Photograph of Faraday-cage-shielded graphene glass, with homogeneous transmittance of ≈80.0% on the entire glass. e,f) Series of Raman spectra from graphene glass in (c,d) along the arrows, with growth time of ≈10 and ≈60 min, respectively. AFM images bordered by green and red frames in (e) show the VG-nanowalls from the regions in corresponding colored squares in (c). The profiles present the different nanowall height of ≈11.6 and ≈47.5 nm, respectively. AFM images bordered by green and red frames in (f) show the LG-layers from the regions in corresponding colored squares in (d). The profiles present the homogeneous thickness of ≈2.2 nm (after transferring onto SiO_2/Si substrate).

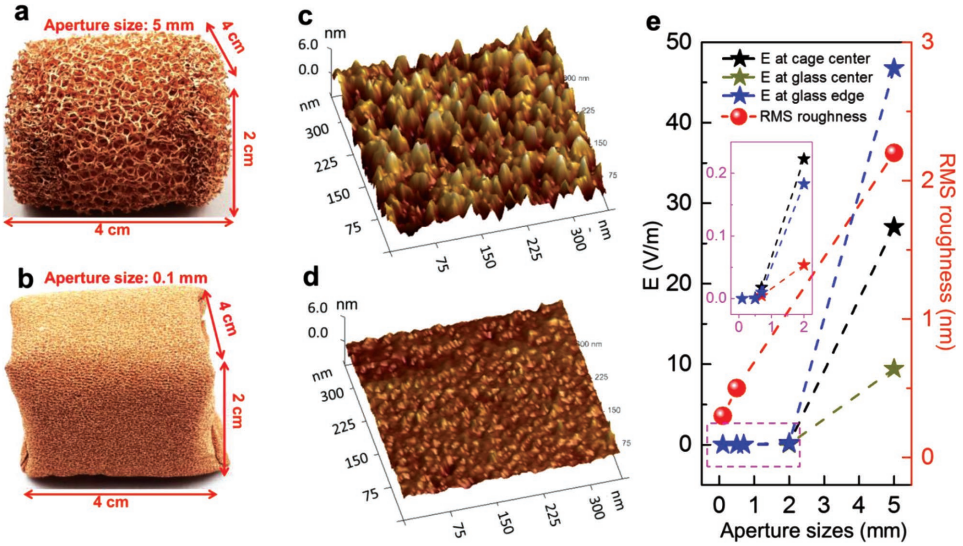

Figure 3. Effects of the aperture size of Faraday cage on the morphology of graphene on glass. a,b) Photographs of Faraday cages (4 cm × 4 cm × 2 cm) constructed with copper foam showing aperture size of ≈5.0 mm a) and ≈0.1 mm b), respectively. c,d) 3D AFM images of graphene on glass obtained in Faraday cages in (a) and (b), respectively. Graphene glasses possess nearly equal transmittances of ≈76.0% and ≈75.5%, respectively. Rough surface with an RMS roughness of ≈2.2 nm and flat surface with a roughness of ≈0.3 nm were observed in (c) and (d), respectively. e) Left axis: Electric field at the cage center, glass center, and glass edge in Faraday cage plotted as a function of the aperture size of the utilized copper foam (≈5.0, ≈2.0, ≈0.7, ≈0.5, and ≈0.1 mm); Right axis: Dependence of RMS roughness of graphene glass on the appetize size of Faraday cage (≈0.1, ≈0.5, and ≈5.0 mm).

presents a nonuniform distribution of graphene thickness at a 10 cm × 6 cm size, with the transmittance varying from ≈30.5% to ≈80.0% as the positions changing from edges to central areas. AFM images bordered by green and red frames in Figure 2e show the density and height difference of VG-nanowalls (≈11.6 vs ≈47.5 nm) at the internal and edge areas of glass, corresponding to the regions in the colored squares in Figure 2c. Additionally, at the central areas, many regions are still void of the coverage of VG-nanowalls. This nonuniformity has also been manifested by a series of Raman spectra in Figure 2e, which present characteristic Raman peaks for graphene at 1349 cm^{-1} (D band), 1591 cm^{-1} (G band), and 2690 cm^{-1} (2D band) (normalized to G peak intensity for comparison). The intensity of 2D peaks increased obviously, as the measured locations approached the edges of glass (red arrows in Figure 2c,e). It is worth noting that such nonuniformity is even inevitable on the small-size graphene glass (1.5 cm × 1.5 cm) (Figure S8a, Supporting Information).

In contrast, for our Faraday-cage-assisted PECVD system, the distortion of the electric field around glass edges is eliminated. This is visually displayed in the 2D electric field simulation (Figure 2b), showing a negligible electric field weaker than 10^{-6} V m^{-1} in the cage (aperture size: 0.1 mm). In this regard, the concentration distribution of carbon cations on substrate surface is relatively even.

Consequently, uniform graphene glass was obtained, with homogeneous ≈80.0% transmittance on entire glass (10 cm × 6 cm, photograph in Figure 2d). AFM images and height profiles in Figure 2f reconfirm the uniformity of LG-layers, with homogeneous thickness of ≈2.2 nm at the internal and edge areas of glass, corresponding to regions in colored squares in Figure 2d (measured after transferring onto SiO_2/Si substrate). The formation of uniform graphene was also convinced by the identical Raman spectra obtained from the entire glass substrates (Figure 2f). In this regard, the Faraday-cage-shielded graphene glass possesses superior uniformity as compared to the normal PECVD-derived one, enabling its scalable applications. However, the quality of the LG-layers is not ideal, which is mainly due to the rather low growth temperature. The crystalline quality could be further improved through increasing the growth temperature, as shown in the selected area electron diffraction and HRTEM images in Figure S9 in the Supporting Information.

The level of shielding effect from Faraday cage could be tailored by adjusting the aperture size of the copper foam. The photographs of the copper-foam-based Faraday cages with the aperture size of ≈5.0 and ≈0.1 mm are displayed in **Figure 3**a,b, respectively. The instructive 2D simulated distributions of electric field in both types of Faraday cages are shown in Figure S11a,e in the Supporting Information, respectively. In the larger-aperture Faraday cage (≈5.0 mm), nonuniform electric field was observed to vary from ≈35 to ≈22 V m^{-1} around the glass surface, thus addressing the not ideal shielding effect. Consequently, discrete graphene flakes, instead of LG-layers, distributed randomly on the glass with a high RMS roughness of ≈2.2 nm (AFM images in Figure 3c and Figure S10a, Supporting Information).

In contrast, in the smaller-aperture Faraday cage (≈0.1 mm), electric field weaker than 10^{-6} V m^{-1} was realized (Figure S11e, Supporting Information). The derived graphene presents a laid-down morphology, featured by a flat surface with an RMS roughness of ≈0.3 nm (Figure 3d and Figure S10b, Supporting Information). Additionally, the 2D simulated distributions of electric field in Faraday cages with the aperture size of ≈2.0, ≈0.7, and ≈0.5 mm are also supplemented in Figure S11 in the Supporting Information. The electric field at the cage center,

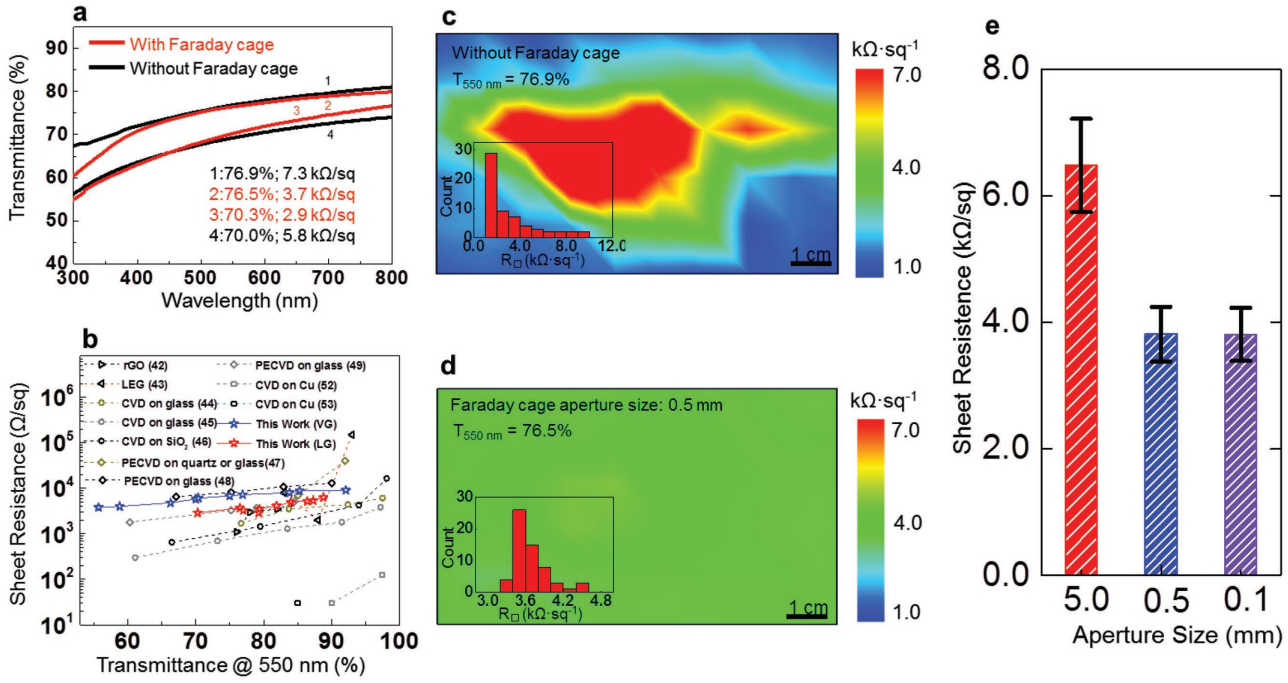

Figure 4. Comparisons of transmittance and sheet resistance of graphene glass fabricated through the normal and Faraday-cage-assisted PECVD routes. a) Transmittance and sheet resistance of normal PECVD-derived (red) and Faraday-cage-shielded graphene glass (≈0.5 mm aperture size) (black). b) Statistics for the transmittance and sheet resistance from 20 graphene glass samples fabricated through the two routes in this work, and the comparisions with the reported results, wherein graphene is synthesized with rGO, LEG, CVD, and PECVD methods. The sheet resistance and transmittance were measured at the central regions of glass. c,d) Spatial distributions of sheet resistance of the two types of graphene glass (nearly equal transmittance: ≈76.9% and ≈76.5%, respectively). The maps are composed of 60 points, collected from 6 cm × 10 cm graphene glass. Insets: Statistical distributions of the sheet resistance. e) Average sheet resistances of graphene glass obtained in Faraday cages with different aperture sizes of ≈5.0, ≈0.5, and ≈0.1 mm.

glass center, and glass edge in Faraday cage plotted as a function of the aperture size intuitively addresses that the smaller aperture size gives rise to a better shielding effect (left axis in Figure 3e). Notably, when the aperture size is up to ≈5.0 mm, the function of Faraday cage starts to be not ideal. The right axis in Figure 3e is the dependence of RMS roughness of graphene glass on the appetize size of Faraday cage. The RMS roughness is obviously increased with enhancing the aperture size.

For transparent electronic applications, the electrical and optical properties of the fabricated graphene glass should be comprehensively evaluated. Similar to other transparent conductive films, the conductivity and transparency of graphene glass present a trade-off effect, varying with the height of graphene nanowall or the layer thickness. The two properties for the normal PECVD-derived graphene glass (black) and the Faraday-cage-shielded one (red) are displayed in **Figure 4**a. Under the identical transmittance at 550 nm, the Faraday-cage-shielded graphene glass showed lower sheet resistance than the normal PECVD-derived one (≈76.5%, ≈3.7 kΩ sq^{-1} vs ≈76.9%, ≈7.3 kΩ sq^{-1}; ≈70.3%, ≈2.9 kΩ sq^{-1} vs ≈70.0%, ≈5.8 kΩ sq^{-1}). The statistics of sheet resistances under various transmittances (Figure 4b) further illustrate the obvious superiority of Faraday-cage-shielded graphene glass in conductivity and transparency. This originates from the weaker carrier scattering and lower light absorption ratio of LG-layers than VG-nanowalls.[25–27] Notably, the sheet resistance and transmittance were measured at the central regions of glass (Figure S12, Supporting Information). Additionally, the statistics also justify our ability to tune the optical and electrical properties of as-fabricated graphene glass. The transmittance and sheet resistance of graphene in the reported systems are also summarized for comparisons. Under the same transmittance, the sheet resistance of LG-layers achieved in this work is comparable, or even lower than that reported previously, wherein the graphene samples were fabricated through PECVD, liquid phase exfoliation from graphite (LEG) or rGO.[42–46] However, the sheet resistance of LG-layers is higher than that of the CVD-grown graphene (growth temperature >1000 °C). This is partially due to the lower growth temperature in this work (≈580 °C) and the relatively lower crystal quality.[47–49] The comparisons of sheet resistance for various types of graphene at ≈80% transmittance (obtained under respective growth temperature) are also presented in Figure S13 in the Supporting Information.[44–53]

Moreover, the Faraday cage design could largely improve the uniformity of sheet resistance of graphene glass, which was clearly reflected in the sheet resistance mapping results in Figure 4c,d (similar transmittance: ≈76.9% and ≈76.5%, respectively). A nonuniform sheet resistance distribution can be observed on the normal PECVD-derived graphene glass (6 cm × 10 cm), with the value varying from ≈7.0 to ≈2.0 kΩ sq^{-1}, as the positions changing from inner areas to the edges (Figure 4c). Notably, this nonuniformity is even inevitable on the small-size graphene glass (1.5 cm × 1.5 cm) (Figure S14a, Supporting Information). In contrast, a homogenous sheet resistance of

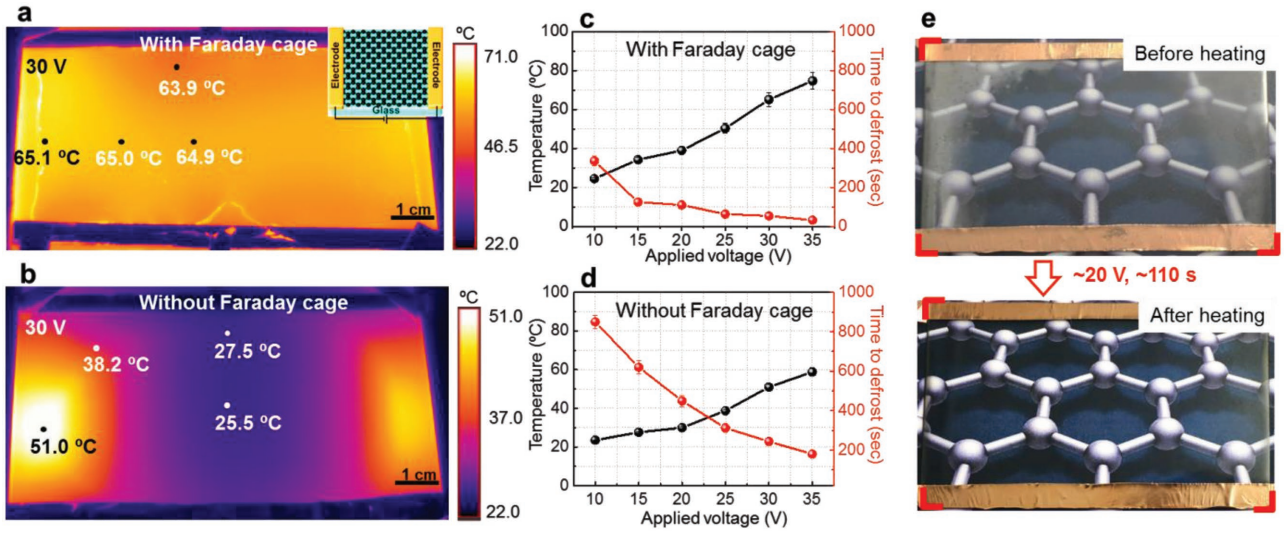

Figure 5. Transparent heating device constructed with graphene glass. a,b) Infrared images of temperature on graphene glass (6 cm × 10 cm) fabricated with the Faraday-cage-assisted a) and normal b) PECVD routes. Inset in (a): Schematic of the graphene glass heater. c,d) Glass temperature and frost removal time plotted as a function of the input voltage for the two types of transparent defrosters. e) Photographs depicting the performance of the transparent defroster device constructed with Faraday-cage-shielded graphene glass, before (upper) and after (lower) heating at ≈20 V for ≈110 s.

≈4.0 kΩ sq^{-1} in 6 cm × 10 cm size can be derived from the Faraday-cage-shielded graphene glass (Figure 4d). The large-scale uniform electrical conductivity of graphene glass holds the promise for its scalable applications in transparent electronics. Additionally, the average sheet resistances of graphene glass obtained in Faraday cages with different aperture sizes of ≈5.0, ≈0.5, and ≈0.1 mm suggest that, a smaller aperture size brings a lower sheet resistance and a better uniformity, as explicitly shown in Figure 4e and Figure S14 in the Supporting Information.

The unique advantages of the Faraday-cage-shielded graphene glass, including its low production temperature, high transparency, reduced sheet resistance, excellent uniformity, and more importantly, its compatibility with normal soda-lime glass, render it readily applicable to the fabrication of transparent heating device, as demonstrated in **Figure 5**a (size: 6 cm × 10 cm, transmittance: ≈72%, sheet resistance: ≈2.9 kΩ sq^{-1}). Inset shows the schematic of the heater. Under the input voltage of ≈30 V, the graphene glass shows uniform temperature distribution of 64.5 ± 1.0 °C, as presented in the IR image in Figure 5a. In contrast, for the heating device constructed with normal PECVD-derived graphene glass, a nonuniform temperature distribution varying from ≈25.5 °C (internal areas) to ≈51.0 °C (edges) was observed under ≈30 V (Figure 5b, transmittance: ≈72% (internal areas), nonuniform sheet resistance: 2.0–6.0 kΩ sq^{-1}). The IR images under ≈20 V further denote the uniformity difference between the two types of samples (Figure S15, Supporting Information). Generally, under various input voltages, the Faraday-cage-shielded graphene glass always enables a higher surface heating temperature than that of the normal PECVD-derived one (left *Y* axes in Figure 5c,d, respectively).

One promising application for the heating performance of graphene glass is to serve as a defroster device (Figure 5e). The device constructed using the Faraday-cage-shielded graphene glass affords an advanced defrosting performance with a completion time of ≈110 s under ≈20 V (right axis in Figure 5c), comparable to that of metal-wire-based defrosting windows utilized in modern vehicles, and superior to the normal PECVD-derived graphene-glass defroster with a completion time of ≈450 s under ≈20 V (right axis in Figure 5d). In general, the Faraday-cage-assisted PECVD method brings large-scale uniformity, good transparency, high heating temperature, and advanced defrosting performance in the transparent heating devices, thus presents potentials in future scalable applications.

In summary, by virtue of the Faraday-cage-assisted PECVD route, the LG-layers were synthesized at a temperature as low as ≈580 °C on a large-size catalysis-free insulating substrate (glass), which is hardly realized through the conventional PECVD method with the typical product of VG-nanowalls, or the thermal CVD method with the necessity of high growth temperature (1000–1600 °C). Considering its low cost, scalable size, high transparency, low sheet resistance, and excellent uniformity, the LG layer-covered glass will favor the next-generation applications in transparent electronics, intelligent building, and advanced optical instruments.

Experimental Section

Synthesis of Graphene on Glass in PECVD: Aixtron Black Magic 6-inch PECVD was used to synthesize graphene on glass. The pressure of the PECVD system is 500 Pa.

Characterization: The prepared samples were characterized using SEM (Hitachi S-4800, operating at 1 kV), Raman spectroscopy (Horiba, LabRAM HR-800, 514 nm laser excitation, 100 × objective lens), contact angle system (DataPhysics, OCA20), UV–vis spectroscopy (Perkin-Elmer Lambda 950 spectrophotometer), and four-probe resistance measuring meter (Guangzhou 4-probe Tech Co. Ltd., RTS-4). The IR image of temperature was obtained by an FLUKE Ti 10 Infrared Camera.

Supporting Information

Supporting Information is available from the Wiley Online Library or from the author.

Acknowledgements

This work was financially supported by the National Key Research and Development Program of China (2016YFA0200103), Beijing Municipal Science and Technology Commission (No. Z161100002116020), the Ministry of Science and Technology of China (2013CB932603), the National Natural Science Foundation of China (51290272, 51432002, and 51472008), the Beijing Municipal Science and Technology Planning Project (Z151100003315013), and the Certificate of China Postdoctoral Science Foundation Grant (2016M590010). J.Y.S. acknowledges the support from Suzhou Key Laboratory for Advanced Carbon Materials and Wearable Energy Technologies, Suzhou, China as well as the support from the Thousand Youth Talents Plan of China.

Conflict of Interest

The authors declare no conflict of interest.

Keywords

Faraday cages, laid-down graphene, plasma-enhanced chemical vapor deposition, vertical graphene

Received: August 24, 2017
Revised: November 15, 2017
Published online: January 10, 2018

[1] J. Kwak, J. H. Chu, J.-K. Choi, S.-D. Park, H. Go, S. Y. Kim, K. Park, S.-D. Kim, Y.-W. Kim, E. Yoon, S. Kodambaka, S.-Y. Kwon, *Nat. Commun.* **2012**, *3*, 645.
[2] J. Chen, Y. Wen, Y. Guo, B. Wu, L. Huang, Y. Xue, D. Geng, D. Wang, G. Yu, Y. Liu, *J. Am. Chem. Soc.* **2011**, *133*, 17548.
[3] J. Hwang, M. Kim, D. Campbell, H. A. Alsalman, J. Y. Kwak, S. Shivaraman, A. R. Woll, A. K. Singh, R. G. Hennig, S. Gorantla, M. H. Rümmeli, M. G. Spencer, *ACS Nano* **2013**, *7*, 385.
[4] M. A. Fanton, J. A. Robinson, C. Puls, Y. Liu, M. J. Hollander, B. E. Weiland, M. LaBella, K. Trumbull, R. Kasarda, C. Howsare, J. Stitt, D. W. Snyder, *ACS Nano* **2011**, *5*, 8062.
[5] J. Sun, T. Gao, X. Song, Y. Zhao, Y. Lin, H. Wang, D. Ma, Y. Chen, W. Xiang, J. Wang, Y. Zhang, Z. Liu, *J. Am. Chem. Soc.* **2014**, *136*, 6574.
[6] J. Sun, Y. Chen, M. K. Priydarshi, Z. Chen, A. Bachmatiuk, Z. Zou, Z. Chen, X. Song, Y. Gao, M. H. Rümmeli, Y. Zhang, Z. Liu, *Nano Lett.* **2015**, *15*, 5846.
[7] X.-D. Chen, Z. Chen, W.-S. Jiang, C. Zhang, J. Sun, H. Wang, W. Xin, L. Lin, M. K. Priydarshi, H. Yang, Z.-B. Liu, J.-G. Tian, Y. Zhang, Y. Zhang, Z. Liu, *Adv. Mater.* **2017**, *29*, 1603428.
[8] M. H. Ruemmeli, A. Bachmatiuk, A. Scott, F. Boerrnert, J. H. Warner, V. Hoffman, J.-H. Lin, G. Cuniberti, B. Buechner, *ACS Nano* **2010**, *4*, 4206.
[9] J. Chen, Y. Guo, L. Jiang, Z. Xu, L. Huang, Y. Xue, D. Geng, B. Wu, W. Hu, G. Yu, Y. Liu, *Adv. Mater.* **2014**, *26*, 1348.
[10] C.-Y. Su, A.-Y. Lu, C.-Y. Wu, Y.-T. Li, K.-K. Liu, W. Zhang, S.-Y. Lin, Z.-Y. Juang, Y.-L. Zhong, F.-R. Chen, L.-J. Li, *Nano Lett.* **2011**, *11*, 3612.
[11] J. Sun, Y. Chen, M. K. Priydarshi, Z. Chen, A. Bachmatiuk, Z. Zou, Z. Chen, X. Song, Y. Gao, M. H. Ruemmeli, Y. Zhang, Z. Liu, *Nano Lett.* **2015**, *15*, 5846.
[12] J. J. Wang, M. Y. Zhu, R. A. Outlaw, X. Zhao, D. M. Manos, B. C. Holloway, *Carbon* **2004**, *42*, 2867.
[13] D. Wei, L. Peng, M. Li, H. Mao, T. Niu, C. Han, W. Chen, A. T. S. Wee, *ACS Nano* **2015**, *9*, 164.
[14] M. Zhu, J. Wang, B. C. Holloway, R. A. Outlaw, X. Zhao, K. Hou, V. Shutthanandan, D. M. A. Manos, *Carbon* **2007**, *45*, 2229.
[15] S. Vizireanu, S. D. Stoica, C. Luculescu, L. C. Nistor, B. Mitu, G. Dinescu, *Plasma Sources Sci. Technol.* **2010**, *19*, 034016.
[16] K. Davami, M. Shaygan, N. Kheirabi, J. Zhao, D. A. Kovalenko, M. H. Rümmeli, J. Opitz, G. Cuniberti, J.-S. Lee, M. Meyyappan, *Carbon* **2014**, *72*, 372.
[17] O. Akhavan, E. Ghaderi, R. Rahighi, *ACS Nano* **2012**, *6*, 2904.
[18] Z. Bo, W. Zhu, W. Ma, Z. Wen, X. Shuai, J. Chen, J. Yan, Z. Wang, K. Cen, X. Feng, *Adv. Mater.* **2013**, *25*, 5799.
[19] S. Mao, Z. Wen, S. Ci, X. Guo, K. Ostrikov, J. Chen, *Small* **2015**, *11*, 414.
[20] A. Garcia-Lekue, T. Balashov, M. Olle, G. Ceballos, A. Arnau, P. Gambardella, D. Sanchez-Portal, A. Mugarza, *Phys. Rev. Lett.* **2014**, *112*, 066802.
[21] H. Ishii, N. Kobayashi, K. Hirose, *Appl. Phys. Express* **2010**, *3*, 5102.
[22] A. W. Tsen, L. Brown, M. P. Levendorf, F. Ghahari, P. Y. Huang, R. W. Havener, C. S. Ruiz-Vargas, D. A. Muller, P. Kim, J. Park, *Science* **2012**, *336*, 1143.
[23] J. Tian, H. Cao, W. Wu, Q. Yu, Y. P. Chen, *Nano Lett.* **2011**, *11*, 3663.
[24] R. R. Nair, P. Blake, A. N. Grigorenko, K. S. Novoselov, T. J. Booth, T. Stauber, N. M. R. Peres, A. K. Geim, *Science* **2008**, *320*, 1308.
[25] H. Ghasemi, G. Ni, A. M. Marconnet, J. Loomis, S. Yerci, N. Miljkovic, G. Chen, *Nat. Commun.* **2014**, *5*, 4449.
[26] X. Hu, W. Xu, L. Zhou, Y. Tan, Y. Wang, S. Zhu, J. Zhu, *Adv. Mater.* **2017**, *29*, 1604031.
[27] Q. Jiang, L. Tian, K.-K. Liu, S. Tadepalli, R. Raliya, P. Biswas, R. R. Naik, S. Singamaneni, *Adv. Mater.* **2016**, *28*, 9400.
[28] M. Cai, R. A. Outlaw, S. M. Butler, J. R. Miller, *Carbon* **2012**, *50*, 5481.
[29] K. Ostrikov, E. C. Neyts, M. Meyyappan, *Adv. Phys.* **2013**, *62*, 113.
[30] K. Yu, P. Wang, G. Lu, K.-H. Chen, Z. Bo, J. Chen, *J. Phys. Chem. Lett.* **2011**, *2*, 537.
[31] M. Hiramatsu, K. Shiji, H. Amano, M. Hori, *Appl. Phys. Lett.* **2004**, *84*, 4708.
[32] J. Zhao, M. Shaygan, J. Eckert, M. Meyyappan, M. H. Ruemmeli, *Nano Lett.* **2014**, *14*, 3064.
[33] X.-D. Chen, Z.-L. Chen, J.-Y. Sun, Y.-F. Zhang, Z.-F. Liu, *Acta. Phys. Chim. Sin.* **2016**, *32*, 14.
[34] A. Malesevic, R. Vitchev, K. Schouteden, A. Volodin, L. Zhang, G. Van Tendeloo, A. Vanhulsel, C. Van Haesendonck, *Nanotechnology* **2008**, *19*, 305604.
[35] K. Ostrikov, I. Levchenko, S. Xu, *Pure Appl. Chem.* **2008**, *80*, 1909.
[36] E. C. Neyts, A. C. T. van Duin, A. Bogaerts, *J. Am. Chem. Soc.* **2012**, *134*, 1256.
[37] H. T. Do, G. Thieme, M. Frohlich, H. Kersten, R. Contrib, *Plasma Phys.* **2005**, *45*, 378.
[38] I. B. Denysenko, S. Xu, J. D. Long, P. P. Rutkevych, N. A. Azarenkov, K. Ostrikov, *J. Appl. Phys.* **2004**, *95*, 2713.
[39] Z. Bo, K. Yu, G. Lu, S. Cui, S. Mao, J. Chen, *Energy Environ. Sci.* **2011**, *4*, 2525.
[40] B. O. Cho, S. W. Hwang, J. H. Ryu, S. H. Moon, *Rev. Sci. Instrum.* **1999**, *70*, 2458.
[41] J.-K. Lee, S.-H. Lee, J.-H. Min, I.-Y. Jang, C.-K. Kim, S. H. Moon, *J. Electrochem. Soc.* **2009**, *156*, D222.
[42] H. A. Becerril, J. Mao, Z. Liu, R. M. Stoltenberg, Z. Bao, Y. Chen, *ACS Nano* **2008**, *2*, 463.
[43] X. Li, G. Zhang, X. Bai, X. Sun, X. Wang, E. Wang, H. Dai, *Nat. Nanotechnol.* **2008**, *3*, 538.
[44] J. Sun, Y. Chen, M. K. Priydarshi, Z. Chen, A. Bachmatiuk, Z. Zou, Z. Chen, X. Song, Y. Gao, M. H. Rümmeli, *Nano Lett.* **2015**, *15*, 5846.

[45] X. D. Chen, Z. Chen, W. S. Jiang, C. Zhang, J. Sun, H. Wang, W. Xin, L. Lin, M. K. Priydarshi, H. Yang, *Adv. Mater.* **2017**, *29*, 1603428.
[46] H. Bi, S. Sun, F. Huang, X. Xie, M. Jiang, *J. Mater. Chem.* **2012**, *22*, 411.
[47] L. Zhang, Z. Shi, Y. Wang, R. Yang, D. Shi, G. Zhang, *Nano Res.* **2011**, *4*, 315.
[48] H. Ci, H. Ren, Y. Qi, X. Chen, Z. Chen, J. Zhang, Y. Zhang, Z. Liu, *Nano Res.* **2017**, https://doi.org/10.1007/s12274-017-1839-1.
[49] J. Sun, Y. Chen, X. Cai, B. Ma, Z. Chen, M. K. Priydarshi, K. Chen, T. Gao, X. Song, Q. Ji, X. Guo, D. Zou, Y. Zhang, Z. Liu, *Nano Res.* **2015**, *8*, 3496.
[50] J. Sun, Z. Chen, L. Yuan, Y. Chen, J. Ning, S. Liu, D. Ma, X. Song, M. K. Psriydarshi, A. Bachmatiuk, M. H. Rummeli, T. Ma, L. Zhi, L. Huang, Y. Zhang, Z. Liu, *ACS Nano* **2016**, *10*, 11136.
[51] H. Medina, Y.-C. Lin, C. Jin, C.-C. Lu, C.-H. Yeh, K.-P. Huang, K. Suenaga, J. Robertson, P.-W. Chiu, *Adv. Funct. Mater.* **2012**, *22*, 2123.
[52] S. Bae, H. Kim, Y. Lee, X. Xu, J.-S. Park, Y. Zheng, J. Balakrishnan, T. Lei, R. H. Kim, Y. I. Song, Y.-J. Kim, K. S. Kim, B. Özyilmaz, J.-H. Ahn, B. H. Hong, S. Iijima, *Nat. Nanotechnol.* **2010**, *5*, 574.
[53] M. Grande, G. V. Bianco, M. A. Vincenti, D. de Ceglia, P. Capezzuto, M. Scalora, A. D'Orazio, G. Bruno, *Sci. Rep.* **2015**, *5*, 17083.